Available online at www.eccomasproceedia.org
Eccomas Proceedia COMPDYN (2023) 2867-2881

ECCOMAS
Proceedia

COMPDYN 2023
9th ECCOMAS Thematic Conference on
Computational Methods in Structural Dynamics and Earthquake Engineering
M. Papadrakakis, M. Fragiadakis (eds.)
Athens, Greece, 12-14 June 2023

IMPROVEMENT OF SEISMIC SAFETY BY LOCAL STRENGHTNING IN ITALIAN PRE-70 RESIDENTIAL RC BUILDINGS DESIGNED FOR GRAVITY LOADS

Santa A. Scala[1], Maria T. De Risi[1], Carlo Del Gaudio[1], and Gerardo M. Verderame[1]

[1] University of Naples Federico II,
Department of Structures for Engineering and Architecture,
{santaanna.scala, mariateresa.derisi, carlo.delgaudio, verderam}@unina.it

Abstract

Pre-code reinforced concrete (RC) buildings in Italy are significantly vulnerable to seismic actions, especially those realized before '70s, since, up to '70, about 85% of the whole national territory was classified as not-seismic prone area. In such areas, buildings were designed to sustain gravity loads only, without capacity design principles, often resulting vulnerable to shear failures both in beams/columns and in beam-column joints under seismic loading. Thus, proper retrofit strategies should be analysed and implemented in order to solve such brittle failures, aiming at improving seismic performance at life safety limit state.
In this work, the seismic assessment of case-study Italian pre-70s RC buildings and the relevant retrofit design are carried out according to the current Italian technical code (D.M.2018). Two case-study residential buildings, designed for gravity loads only and different for number of stories, are analysed to assess their "as-built" capacity. The latter is compared with the seismic demand at the life safety limit state, considering all Italian municipalities classified as not-seismic area up to '70 as possible building locations. Thus, for each building/site, the capacity-to-demand ratio, is evaluated. Then, local strengthening interventions (wrapping with Fiber Reinforced Polymers strips for beams/columns and CAM® technology for joints) are designed aiming at the complete resolution of the detected shear failures. The post-strengthening seismic capacity is compared to seismic demand to finally quantify the effectiveness of such a local intervention depending on the building height and the current seismic hazard throughout the Italian country.

Keywords: Existing buildings; seismic capacity; reinforced concrete; retrofit; shear failures; local strengthening.

ISSN:2623-3347
Peer-review under responsibility of the organizing committee of COMPDYN 2023.
doi: 10.7712/120123.10606.21273

1 INTRODUCTION

In areas prone to earthquakes, existing reinforced concrete (RC) buildings are often vulnerable to seismic loading and require retrofitting strategies and mitigation policies to ensure reliable seismic performance assessment and risk mitigation. Pre-code or low-code RC buildings present different failure typologies compared to newly designed buildings [1] and need to be considered for retrofitting. This is certainly true for RC buildings in Italy constructed before the 1970s [1], which often exhibited shear failures in beams/columns and beam-column joints after earthquakes. In the past 50 years, the Italian government has spent a significant amount (an annual cost of about four billion euros actualized to 2019) of money on direct and indirect costs due to earthquakes, half of which was related to assistance, recovery, and post-event reconstruction for residential buildings [2]. Therefore, a large-scale seismic strengthening intervention plan for those buildings is necessary to drastically reduce seismic losses and casualties in future events.

The primary aim of retrofitting is life safety prevention, which can be achieved through three main approaches according to the Italian code, D.M. 2018 [3]: achieving the new-design building safety level, improving the as-built safety level by a certain percentage, or with local strengthening interventions that do not change the lateral stiffness of the structure, producing an improvement of the seismic response of the involved primary elements.

This study presents the as-built assessment of Italian pre-70 RC buildings (characterized by different number of storeys) in about 6700 municipalities, characterized by different seismic hazard. The seismic capacity of each building/site has been evaluated at *Severe Damage* (SD) Limit State (LS) in a code-based approach according to Italian seismic prescriptions ([3], in tune with CEN, 2005, [4]). Retrofitting has been designed to solve the shear failures at SD LS in a local strengthening intervention approach, with post-strengthening seismic capacity compared to seismic demand to quantify the effectiveness of the intervention depending on building height and seismic hazard.

2 CASE STUDY BUILDINGS

This study focuses on a sample of Italian reinforced concrete (RC) buildings constructed before 1970, which are intended to represent most of the RC buildings built during this period. In fact, according to ISTAT 2011 [5], Italy has approximately 3.6 million RC buildings throughout the country, with about 1.1 million constructed before 1970. At this time, approximately 85% of the national territory (equivalent to about 6700 municipalities) was classified as a "non-seismic prone" area (see Figure 1). Despite this classification, several strong earthquakes have affected Italy in the last century, resulting in significant losses of life and damage to buildings. In response to these events, seismic hazard classification has been revised several times over the past century. Currently, the sites that were not considered to be seismic-prone until the 1970s are classified according to the hazard map shown in Figure 1, which divides Italy into four "seismic zones" based on the expected value of acceleration on stiff soil with a 10% probability of exceedance in 50 years. It should be noted that only 2% of the considered municipalities are in the first seismic zone (SZ1), while most of them (about 52%) are in the third seismic zone (SZ3). The remaining municipalities are almost equally distributed between the second (SZ2, 23%) and the fourth (SZ4, 17%) SZ.

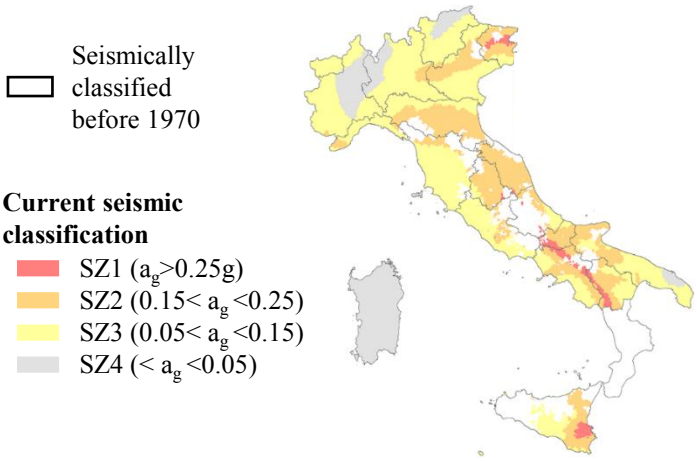

Figure 1. Current Italian seismic classification (based on acceleration on stiff soil a_g with 10% probability of exceedance in 50 years) of municipalities not classified in 1970.

Accordingly, the large majority (88%) of reinforced concrete structures built before 1970 were designed to withstand only gravity loads, even though the current seismic classification acknowledges the need to consider seismic action. The case-study buildings selected for analysis in this study are two RC residential buildings with the same floor plan (approximately 200 m^2), but with different numbers of stories (3 and 6 stories), both designed according to the obsolete technical code in force in Italy until 1970 (Royal Decree, R.D. 1939, [6]).

Both the case-study buildings use the same moment resisting frames (MRFs) system, shown in Figure 2a. This system relies on parallel 2D resisting frames in the longitudinal (X) direction only, which was typical in pre-1970 reinforced concrete buildings in Italy.

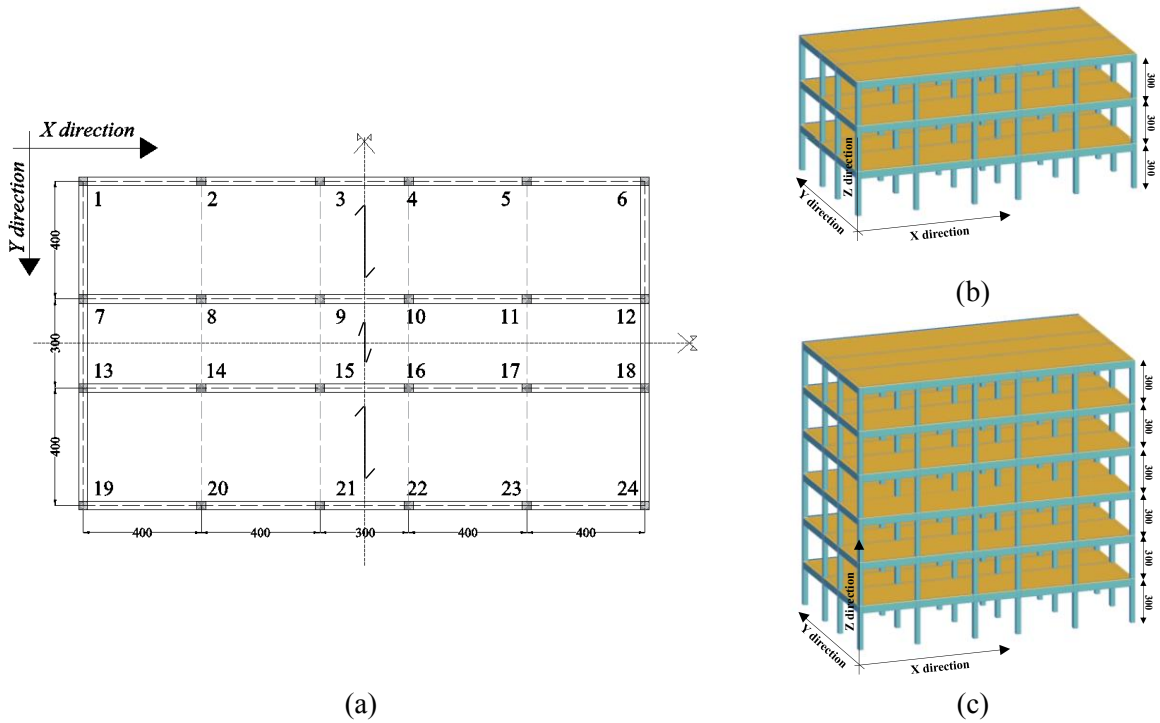

Figure 2 Plan (a) and 3D (b-c) views of analyzed case-study buildings. (Dimensions in centimeters)

Beams connecting columns in the transverse (Y) direction are absent, except for along the exterior perimeter. The floorplan, shown in Figure 2a, is symmetrical in both the main perpendicular directions (X and Y), with an interstory height of 3 meters (Figure 2b-c).

The *maximum allowable stress* method, adopted according to the Italian code in force until the construction time [6-7], assumes a maximum allowable stress of 5 or 6 MPa for concrete (in case of purely compressive loads or bending actions, respectively), and 140 MPa for reinforcing bars. Additionally, plain bars made of *AQ42* steel typology are assumed, which was typical during the reference period in Italy [8]. Design loads and infill weight are the same used in [9].

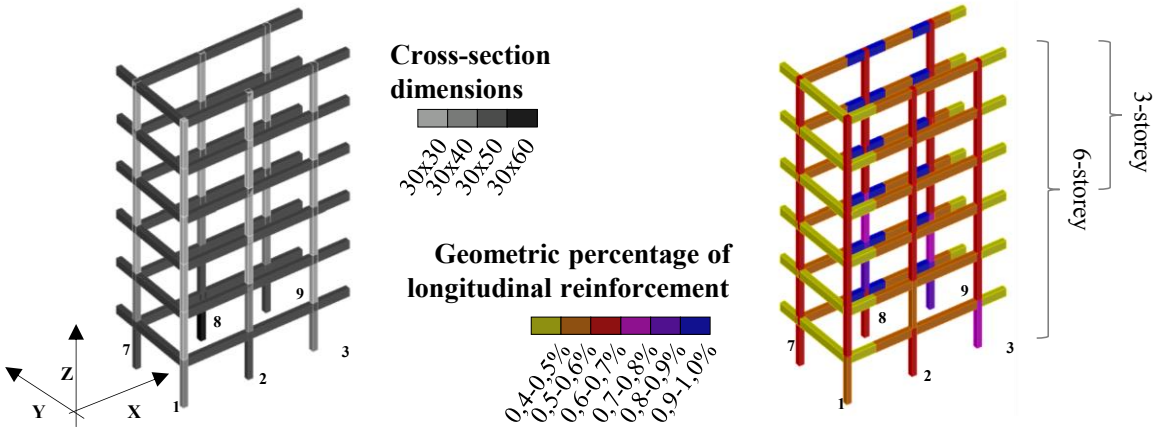

(a) (b)

Figure 3 Cross-section dimensions (a) and geometric percentage of longitudinal reinforcement (b) resulting from simulated design.

Figure 3 presents the main outputs of the simulated design, including resulted cross-sections (Figure 3a) and geometrical percentage of longitudinal reinforcement ρ (Figure 3b) for ¼ of the whole structures, relying on its double-plan symmetry. It should be noted that the simulated design of 6-storey buildings allows obtaining the cross-section dimensions and reinforcement details also for 3-storey case-study building. In fact, the 3-storey building matches the upper 3 storeys of the 6-storey building.

All beams have a 30×50 cm^2 cross-section, whereas column sections vary from a minimum of 30×30 cm^2 (for the upper storeys) to a maximum of 30×60 cm^2 (for central columns of the ground floor). Interior longitudinal beams have the highest ρ values (about 1%) since the floor weight is sustained by the longitudinal frames only. The minimum value of ρ (i.e., about 0.4%) characterizes the beams in the transverse direction. The reinforcement ratio in the columns decreases moving from the ground floor ($\rho \approx 0.9\%$) to the upper stories ($\rho \approx 0.6\%$). Stirrups with 140 mm spacing and 6 mm diameter are used in columns, complying with the minimum amount of transverse reinforcement required by the technical code in force in the considered time period [6, 1]. Stirrups with 250 mm spacing and 8 mm diameter characterize all beams, except for interior ones in the longitudinal direction, where 75 mm spacing is adopted at the beam ends.

3 ITALIAN CODE-BASED SEISMIC ASSESSMENT

This section shows the code-based assessment of "as-built" case-study buildings according to the current Italian code (D.M. 2018) via pushover (PO) analysis within the N2 framework [10]. Case-study buildings described above are located in the centroids of each Italian munic-

ipality classified as not-seismic prone area before ’70, also taking into account the current soil typology [11, 3, 4].

According to D.M. 2018 the code-based assessment at a given limit state (LS_i) can be expressed through the synthetic parameter ζ_e index, defined as the capacity-to-demand ratio generally calculated in terms of peak ground acceleration (PGA):

$$\zeta_e(LS_i) = \frac{PGA_C(LS_i)}{PGA_D(LS_i)} \quad (1)$$

where PGA_C is the seismic capacity at a given limit state, obtained assuming a *Full Knowledge Level, KL* [3, 4], since the mean values of mechanical properties are used for capacity calculations without any further reduction. PGA_D is the seismic demand at the same limit state, obtained considering both the site hazard on stiff soil and the site effects due to soil amplification (since a plan topography is always assumed).

Lastly, the seismic assessment is performed considering the *Severe Damage* (SD) limit state [3, 4], corresponding to seismic actions with a return period (T_R) of 475 years. The SD limit state is reached when for the first time a flexural or a shear failure occurs. In particular, as suggested by the Italian prescriptions, the ductile failure at SD LS is assumed to occur when the chord rotation demand reaches ¾ of the ultimate chord rotation capacity (calculated according to [12]. Joints shear failure occurs when its principal compressive stress overcomes 0.5fc (JF(C)), or if the principal tensile stress overcomes 0.3 √ fc (JF(T)). Lastly, columns/beams shear failure occurs when the shear demand overcomes the shear strength, the latter evaluated according to the model of [3, 13].

3.1 Modelling assumptions

The seismic response of the case-study buildings was numerically reproduced using the OpenSees platform [14]. To achieve this, each building was modelled as a 3D bare model, with infills modelled only in terms of masses and loads, as common in practice-oriented code-based assessment.

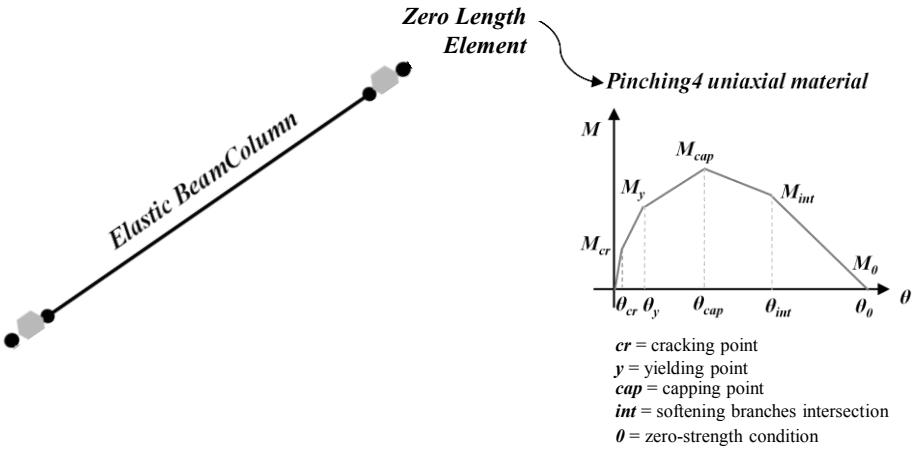

Figure 4. Adopted lumped plasticity approach implemented in OpenSees using elastic *BeamColumn Elements* in series with *Zero-Length Elements* located at each beam/column end and characterized by the *Pinching4* uniaxial material to reproduce the Verderame and Ricci (2018) flexural response.

The floors were assumed to be stiff in their own plane, while the joints' nonlinear response was not numerically reproduced, assuming them as rigid elements. The primary elements (beam/columns) were modelled as ductile elements, with only the nonlinear flexural response

being reproduced in the numerical model. Thus, any eventual shear failures in the columns, beams, or joints were detected by post-processing the static pushover results, which is also a common practice. To model the flexural response of the RC beams and columns, a lumped plasticity approach was used (as shown in Figure 4). This approach assumed a shear length equal to half the element length and adopted a moment-chord rotation (M-θ) relationship of [15], specific for RC elements with plain bars.

3.2 Static PO outcomes

Nonlinear static pushover analyses were conducted for each building in both longitudinal and transverse directions, using two different lateral load distributions as specified by [3]: *(i)* "modal" distribution, which was proportional to the first vibration modal shape in each direction, and *(ii)* "uniform" distribution, which was proportional to the storey horizontal accelerations. The resulting capacity curves are shown in Figure 5(a-b) in terms of spectral displacement (S_d) and spectral pseudo-acceleration ($S_a(T)$), along with the corresponding collapse mechanisms for each direction/load distribution.

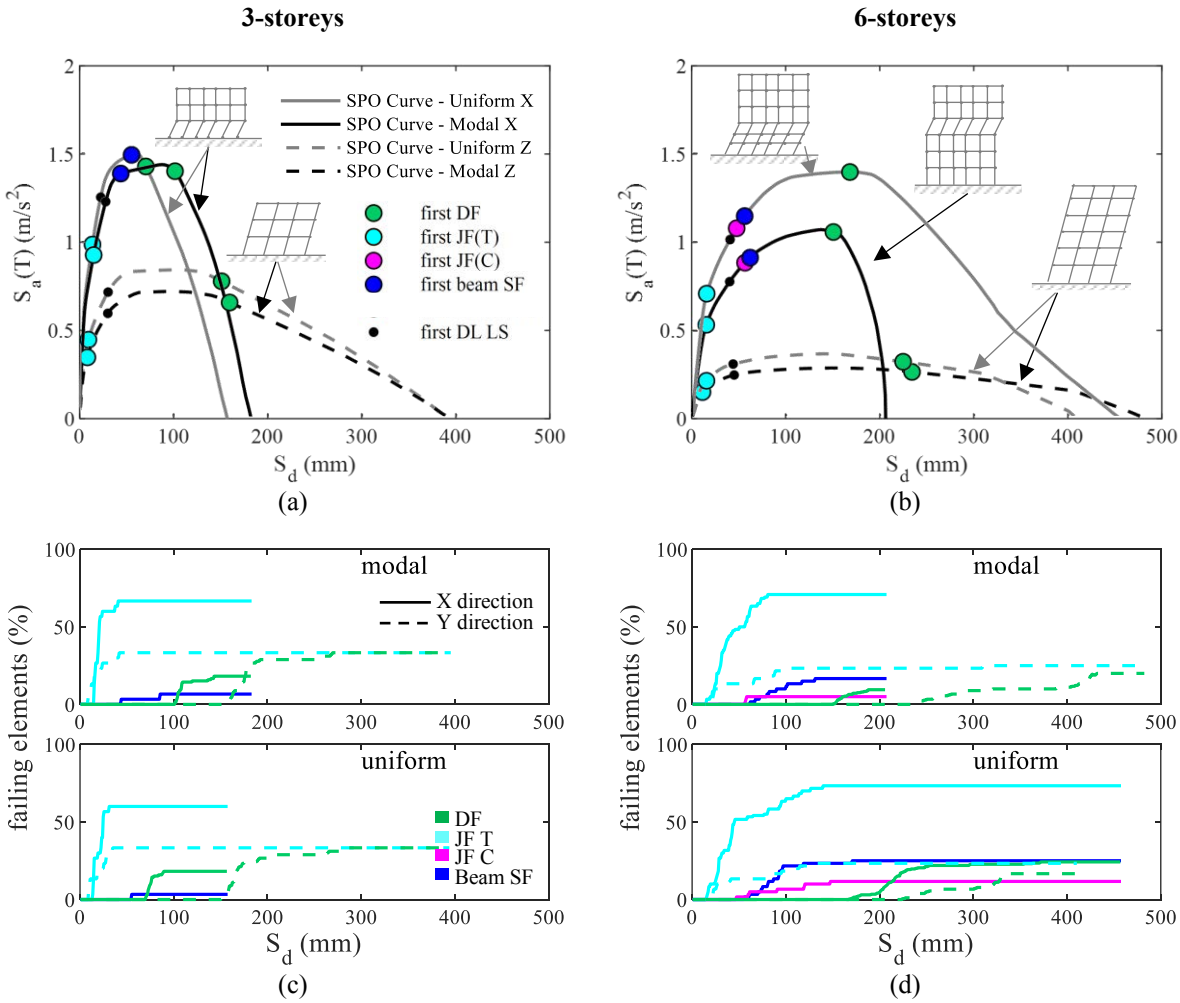

Figure 5 Capacity curves with relevant collapse mechanisms (a-b) and evolution of the considered failure typologies at SD LS (c-d) for both case-study buildings, both direction and load distributions.

A global collapse mechanism is observed in the transverse direction for both the case-study buildings and for both the lateral load patterns, whereas local mechanisms are observed in the longitudinal direction. In particular, for the 3-storey building local first-floor mechanisms is

observed applying both the load distributions; for 6-storey building a fourth floor and a pseudo-global mechanism are observed when modal and uniform distribution are applied, respectively. Moreover, each capacity curve shows the achievement of the first tensile (T) or compression (C) joint failure (JF), the first shear failure (SF) in beams or columns, the first ductile failure (DF), and also the capacity point at the Damage Limitation (DL) LS. The latter is assumed to be achieved when for the first time an inter-story drift ratio equal to 0.5% is achieved. It should be noted that JF(T) are exhibited (in both directions) by all case-study buildings, whereas only the tallest one (6- storey building) also shows JF(C) (only in the X direction). Beams SFs occur in X direction in each analyzed building, conversely columns SF is never observed.

Moreover, Figure 5(c-d) shows the percentage of failing elements in each pushover analysis step for both load distributions and directions. Going from the 3- to 6-storey building, the maximum percentage of JF(T) increase in the X direction, reaching about 75%. The percentage of JF(C) in the 6-storey building does not exceeds the 10% of the total number of beam-column joints, and the maximum percentage of beams SFs increases with the number of storeys, reaching about the 25%. DFs happen in less than 50% of the elements, mostly in the Y direction.

3.3 Safety index assessment

At each LS_i the safety index ζ_e (as defined in Eq. 1) can be calculated. To obtain such result, starting from the capacity curves of Figure 5(a-b), first the equal-energy approach suggested by D.M. 2018 is applied, bi-linearizing each curve up to 85% of the peak load. In Figure 6(a), such procedure is shown for a single curve, for sake of example: an Elastic-Perfectly-Plastic (EPP) idealization is obtained, defining the elastic branch by the capacity curve point at 60% of the peak load.

As shown in Figure 6(a), the slope of this latter branches provides the effective period T_{eff} (namely, 0.77-0.70 s in X direction and 1.11-1.00 s in Y direction for modal-uniform distribution respectively in 3-storey building; 1.23-1.07 s in X direction and 1.93-1.68 s in Y direction for modal-uniform distribution respectively in 6-storey building).

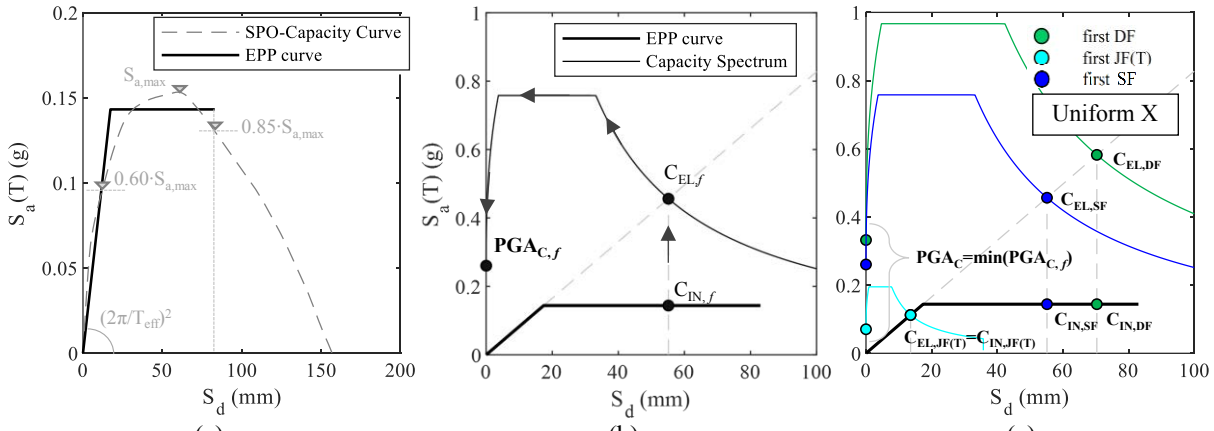

(a) (b) (c)

Figure 6 From capacity curve to EPP idealization (a); from EPP idealization to a capacity spectrum for a given f failure inelastic point (b); PGAC evaluation at the *SD* limit state (c), for a given site. (Case: 3-storey building in Uniform X distribution/direction).

In Figure 6(b), with reference to a given *f* failure, the corresponding capacity spectrum is obtained, first going from the inelastic capacity point, $C_{IN,f}$, to the elastic one, $C_{EL,f}$, by using

the R-μ-T relationship by [16, 3]. Then, the spectrum passing by $C_{EL,f}$ point is identified by a logarithmic interpolation among the nine spectra provided by code (with T_R ranging from 30 to 2475 years).

Such procedure is shown in Figure 6(c) for each failure occurred in the 3-storey buildings in Uniform X distribution/direction, for a given site. In fact, the first achievement of each failure (i.e., the first tensile joint failure, the first shear and ductile failure in a primary element) are reported on obtained EPP curve, given the corresponding spectral displacement S_d (i.e., $C_{IN,JF(T)}$, $C_{IN,SF}$, and $C_{IN,DF}$ respectively). Thus, the R-μ-T relationship allows going from inelastic to corresponding elastic points (i.e., $C_{EL,JF(T)}$, $C_{EL,SF}$, and $C_{EL,DF}$), then logarithmic interpolation allows moving from such elastic points to the relevant PGA values (i.e., $PGA_{C,JF(T)}$, $PGA_{C,SF}$, and $PGA_{C,DF}$ respectively). Thus, the PGA_C for a given load distribution and direction is the minimum among all the obtained $PGA_{C,f}$ values (Figure 6(c)).

Moreover, the minimum of all values (derived for a given distribution/direction) is the building capacity in the as-built condition ($PGA_{C,\,ante}$) at the considered limit state, based on which the safety index is evaluated. Conversely, the seismic demand (PGA_D), at the same limit state, is obtained for each considered site by means of the pseudo-acceleration spectrum associated to the corresponding T_R.

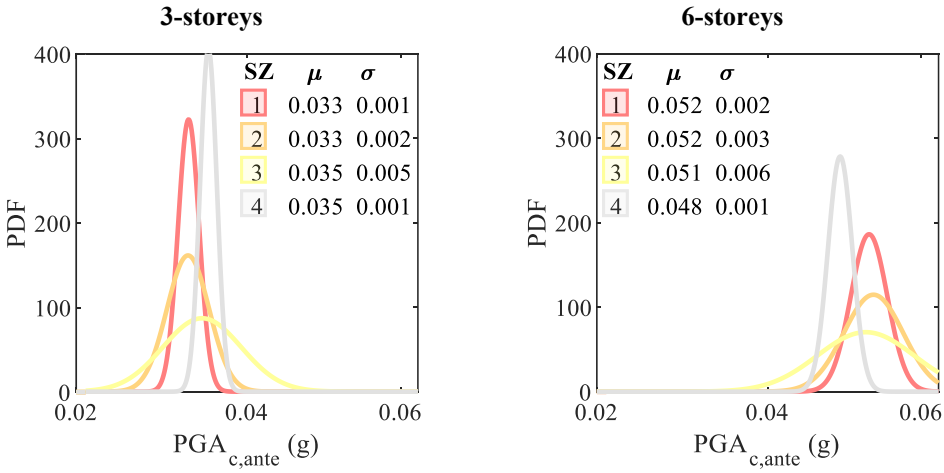

Figure 7. PDF of $PGA_{C,ante}$ at the Sever Damage (SD) limit state for 3- and 6-storey buildings.

Figure 7 shows the probability density function of as-built $PGA_{C,ante}$, at SD LS, thus obtained, fitted with a gaussian distribution, for all the considered sites, distinguishing for seismic zone (ZS), along with the associated mean (μ) and standard deviation (σ) values. It can be noted that, $PGA_{C,ante}$ is always very low, since it is always associated to the first JF(T) and to a capacity T_R lower than 30 years. μ values of $PGA_{C,ante}$ range from 0.03g to 0.05g, slightly increasing from 3- to 6-storey buildings. For each building, σ values are always higher for ZS3 (i.e., the most populated ZS).

In Figure 8, $\zeta_{e,ante}$ indexes are shown as a function of PGA_D for each analysed building, distinguishing in the current four SZs (see Figure 1(b)). The safety index is always lower than 1, except than for a very limited number of 6-storeys buildings located in ZS4. A decreasing trend is observed increasing the seismic demand (namely, going from the fourth to the first ZS), regardless of the number of storeys.

The fitting curve describing such decreasing trend is reported in Figure 8 following the functional law $aPGA_D^b$, where *a* and *b* are regression coefficients changing with the number of storeys. The obtained curves provide the expected $\zeta_{e,ante}$ value, given the seismic demand, for the Italian residential RC buildings designed between '50 and '70 for gravity loads only.

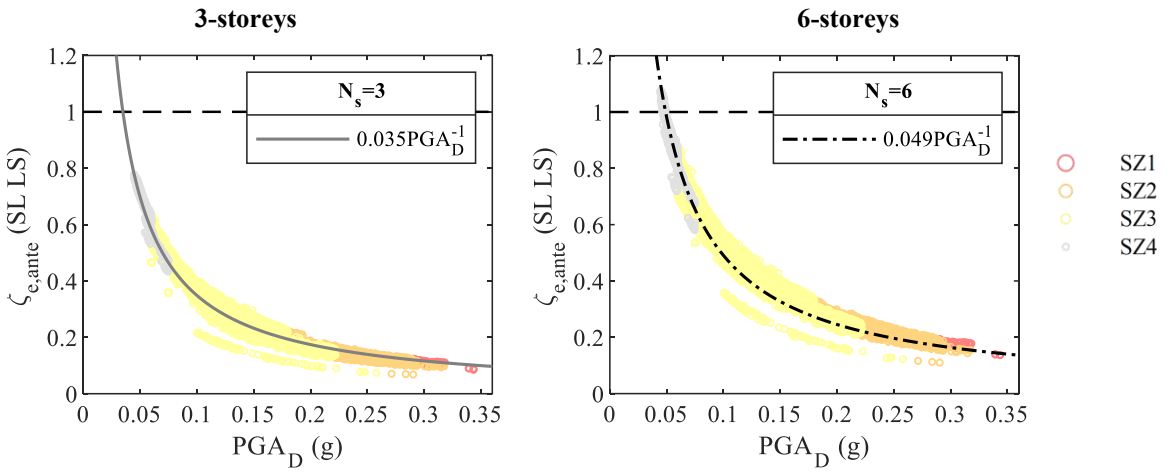

Figure 8. As-built safety index at the Sever Damage (SD) limit state for 3- and 6-storey buildings.

Thus, such mean curves could greatly shorten the time/effort for the seismic assessment of buildings like those analysed herein, directly providing the expected safety index (in KL3), starting from the seismic demand. Parameters *a* and *b* are reported in Figure 8 for each building. It is worth noting that, since the parameter *b* is equal to 1 for all buildings, *a* parameter actually represents the expected value of $PGA_{C,ante}$ at SD LS.

4 RETROFITTING STRATEGY

In the previous section, the building's seismic assessment has been performed, according to the normative prescriptions, thus leading to the definition of the safety index $\xi_{e,ante}$ at the *LS* limit state. In this section, the adopted retrofit strategy and the chosen techniques to increase $\xi_{e,ante}$ are explained. Thus, the retrofit design and the relevant ξ_e increment are provided.

4.1 Local interventions and adopted retrofit strategies

In this work, an approach based on increasing building capacity (i.e., PGA_C) through local strengthening is adopted in order to improve the *ante-operam* safety index. In fact, shear failures can be solved using Fiber Reinforced Polymers (FRP) wrapping for shear-sensitive elements [17, 18, 19, 20] and CAM® technology [20, 21, 22, 23] for tensile failure of joints. The target is to solve shear failures at the plastic shear demand (modifying the shear-sensitive elements in ductile members), without modifying the pushover curve or seismic demand.

More in detail, to solve joints (tensile) failures, CAM® technology [22, 23] is adopted herein, relying on the use of pre-stressed steel strips confining the joint core [21]. The number of pre-stressed steel strips is designed by means of the "post-cracking" approach, according to [21] (in tune with [3, 4] for newly designed reinforced joints), thus considering steel strips as additional transverse reinforcement within the joint region. Joint shear demand is evaluated as the maximum tensile demand deriving from converging beams minus the shear load carried by the diagonal compressed concrete strut within the joint core [3, 4, 21].

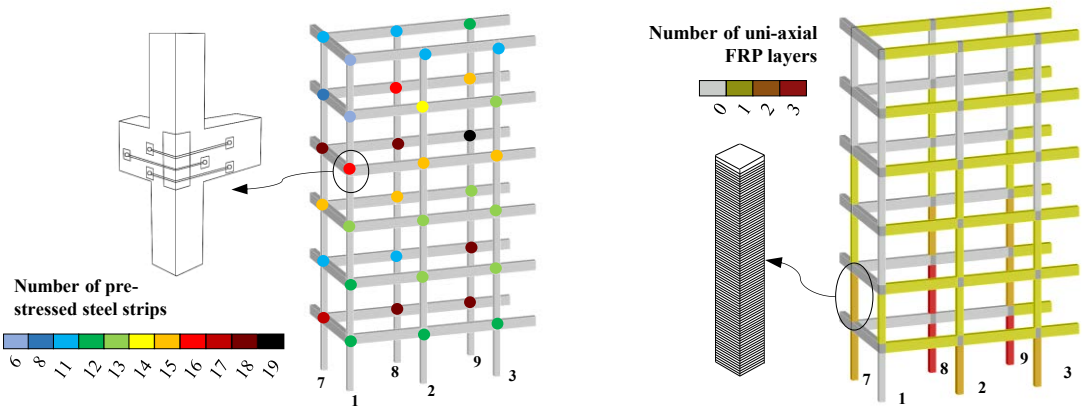

(a) (b)

Figure 9. Number of pre-stressed steel strips for beam-column joints (a); number of uniaxial FRP layers (b).

Figure 9 shows strengthening design outcomes for all shear-sensitive elements, detected by means of a-priori classification. In particular, Figure 9(a) provides the resulting number of pre-stressed steel stirrups for each (T-)shear sensitive joint, assuming a nominal yield strength equal to 400 MPa and a transverse section of 0.9×19 mm^2 [21]. Note that Figure 9 shows the design outputs for ¼ of the whole structure only, due to the plan symmetry in both directions, as already observed above. The maximum number of required steel strips is 19, thus making the designed intervention on joints feasible by distributing the obtained strips in 3 layers along beams height (as shown in Figure 9(a)). Moreover, the shear strengthening of beams and columns is designed, by using a uniaxial carbon fibre polymer whit high elastic modulus (230 GPa) and an equivalent thickness equal to 0.166 mm. The shear capacity of FRP-strengthened elements is evaluated according to CNR-DT 200/2004 [24]. For columns, wrapping on 4 sides is designed, along the whole column height; the resulting number of FRP layers is shown in Figure 9(b) for each shear-sensitive column. For all shear-sensitive beams, only one layer (in U-shape configuration) is sufficient, regardless of the number of stories, extended to the beams ends, ranging from the 14% to the 50% of the whole beam length, depending on the considered beam.

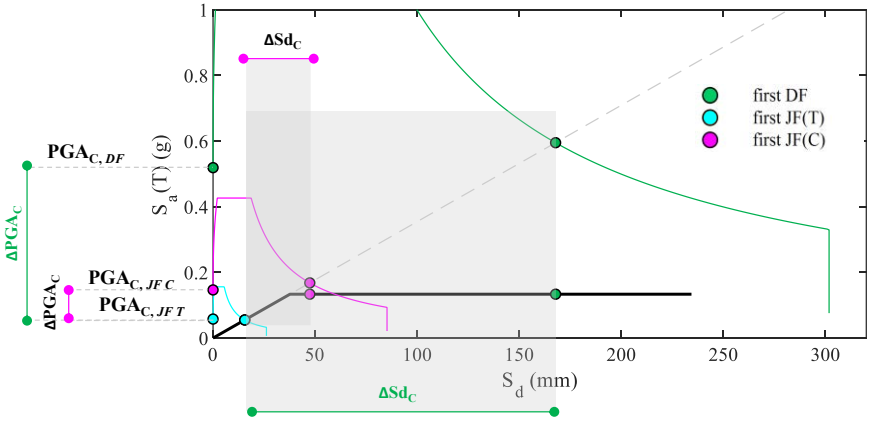

Figure 10. Seismic capacity increment at SD LS in terms of S_d ($\Delta S_{d,c}$) and PGA_C (ΔPGA_c) moving from as-built to post-retrofit condition in presence (magenta marked) or absence (green marked) of JF(C) failures.

If any seismic analysis was performed, the local intervention should involve all shear sensitive elements, as in Figure 9. On the contrary, based on the SPO results shown in Figure 5(a-

b), the strengthening intervention can be optimised aiming at increase the seismic capacity from the first JF(T) (which always limits the as-built performance) ($PGA_{C,JF\,(T)}$) to the first DF ($PGA_{C,DF}$) (as shown in Figure 10 by means of green lines). To this aim, the retrofit can be limited to the shear-sensitive elements that actually exhibit a shear failure during the pushover analyses between the first JF(T) and the first DF, deriving the number of such failing elements from failure mapping of Figure 5(c-d). As a result, building PGA_C can increase by ΔPGA_C (being the same the pushover curve in *ante-* and *post-operam* condition) and, in tune, the safety index increases. Nevertheless, it is worth noting that JF(C), if any, cannot be solved by means of local strengthening interventions, limiting the efficiency of the adopted strategy. If JF(C) occurs before the first DF, a limited ΔPGA_C can be obtained (Figure 10, magenta lines). Such circumstance occurs for the tallest building analysed here (6-storey building), reducing the maximum potential ΔPGA_C by 60%. Thus, in the post-retrofit phase, the seismic capacity is equal to that at the first DF for 3-storeys building, maximizing the effectiveness of the selected retrofit strategy. For 6-storey case-study building, the local strengthening leads to a displacement capacity equal to that at the first JF(C). In summary, the selected strengthening strategy allows increasing building displacement and, in tune, PGA capacity at SD LS from the first JF (T) to the minimum between the first DF and the first JF(C).

4.2 Safety index for retrofitted buildings

The safety index is re-assessed after the implementation of local strengthening, based on the same pushover curves of Figure 5a, for all the considered sites in Italy.

Figure 11 shows the PDF of PGA_C at SD LS (fitted with a gaussian distribution) of post-retrofit buildings for all the considered sites, distinguishing for ZS. The increment of PGA_C with respect to the as-built condition is very high for the lowest building, when JFs(C) do not occur at all: μ values of $PGA_{C,post}$ result about 9.7 times higher, for 3-storey buildings, than the as-built condition (averaging among all SZs). On the other hand, for the tallest building, such an increment is more limited: μ values of $PGA_{C,post}$ result 3.1 times the $PGA_{C,ante}$ for 6-storey buildings (averaging among all ZSs), due to the occurrence of JF(C) before DFs. For each building, σ values are always higher for ZS3 (i.e., the most populated ZS) also in post-retrofit condition, and, generally, given the ZS, they are higher for the post-retrofit condition with respect to as-built phase (except than for ZS1).

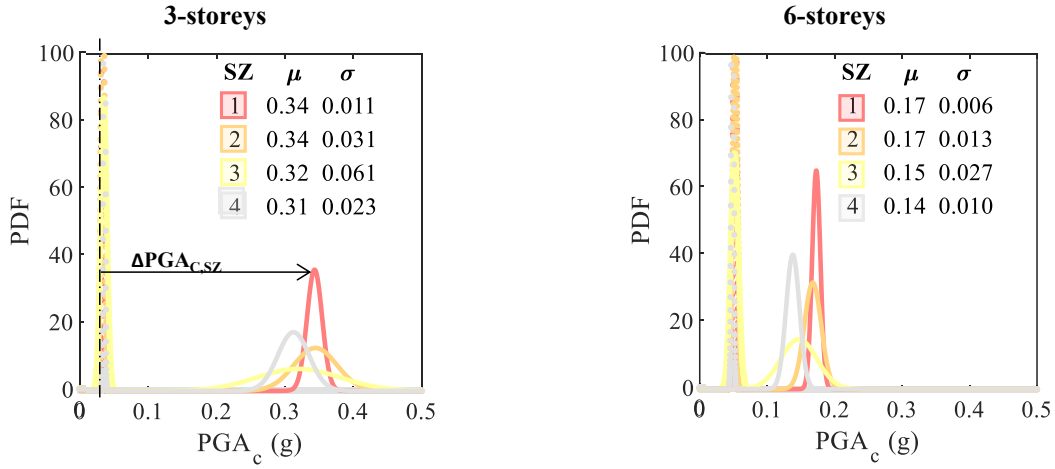

Figure 11. PDF of $PGA_{C,post}$ at the Sever Damage (SD) limit state for 3- and 6-storey buildings

In Figure 12(a-b), the safety index increment at SD LS, $\Delta\zeta_e$, (= $\zeta_{e,post}$- $\zeta_{e,ante}$) is provided, for each case-study buildings, showing its trend with the seismic demand expressed in terms of

PGA$_D$. Such $\Delta\zeta_e$ represents the maximum increment of $\zeta_{e,ante}$ that can be achieved with the selected retrofitting.

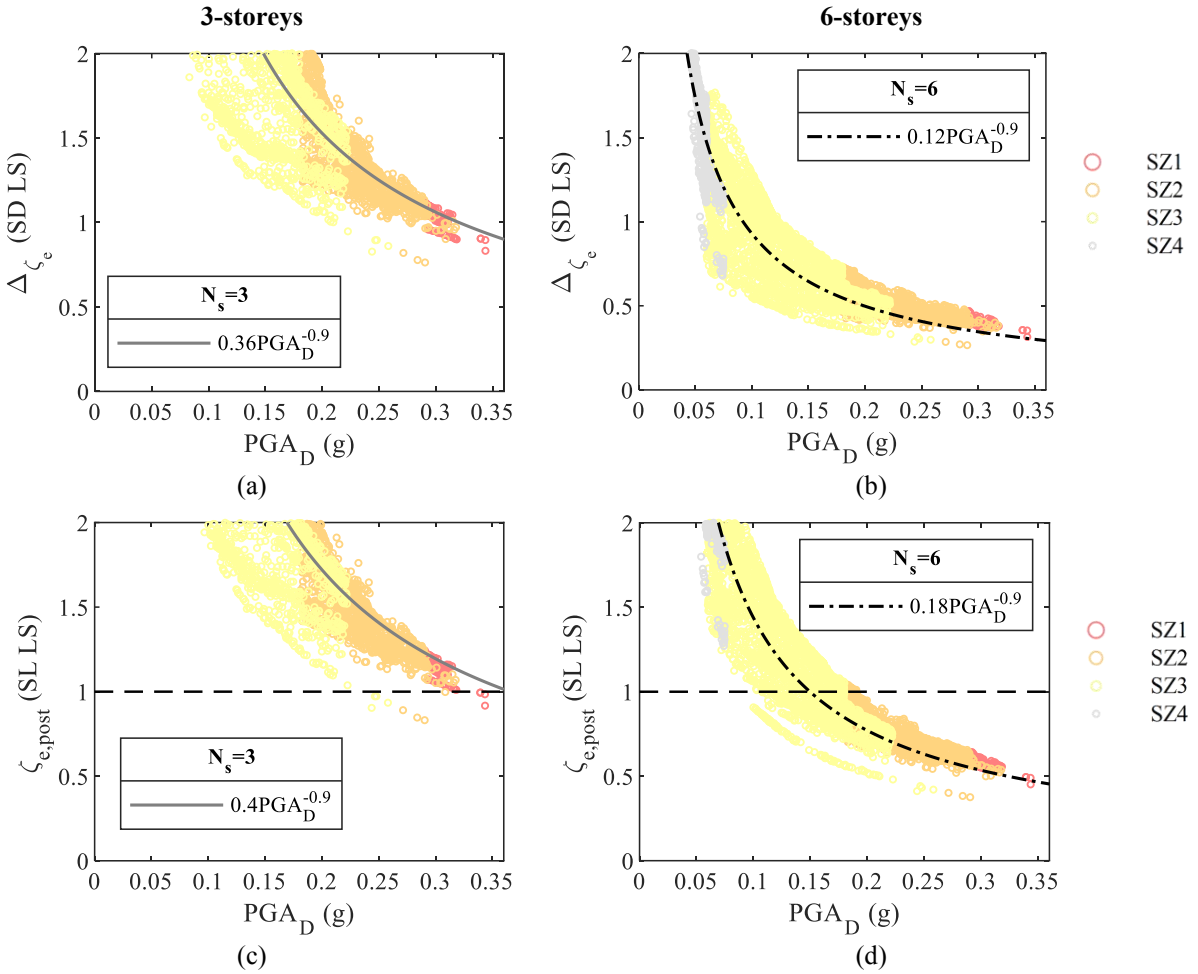

Figure 12. Safety index increment (a-b) and safety index in the post-operam condition (c-d) at SD LS.

Additionally, both the safety index increment at SD LS $\Delta\zeta_e$ (= $\zeta_{e,post}$ - $\zeta_{e,ante}$) and the relevant index in the post-operam condition ($\zeta_{e,post}$), show a decreasing trend, increasing the seismic demand. Fitting parameters for both $\zeta_{e,post}$ and $\Delta\zeta_e$ are reported in the relevant plot (see Figure 12).

Significant increments in ζ_e can be observed (Figure 12), especially in low-medium hazard sites (i.e., ZS3 and ZS4) and especially for 3-storey buildings, where there isn't any limitation due to JFs(C), as observed above.

In particular, the retrofitted 3-storeys building shows $\zeta_{e,post}<1$ only in the 0.2% of the sites (for high-medium hazard sites, ZS1 and ZS2), always reaching at least $\zeta_{e,post}=0.6$ (being the latter a threshold for seismic upgrading of strategic buildings). As expected, for the taller building (6-storeys ones), the occurrence of JFs(C) limits the $\Delta\zeta_e$ increment (Figure 12): the percentage of sites with $\zeta_{e,post}<1$ significantly increases (37%, mainly in ZS1,2,3) (Figure 12(c-d)). Moreover, $\zeta_{e,post}$ values can result even lower than 0.6 (5% of sites), especially for high-medium hazard sites.

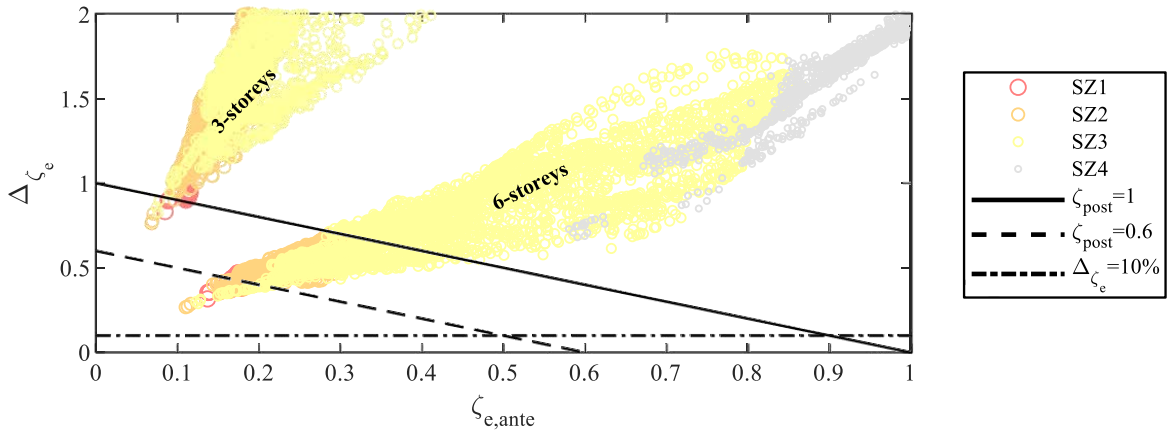

Figure 13. Safety index increment at SD LS versus the relevant as-built safety index for both case-study buildings.

However, the adopted intervention strategy always allows obtaining at least an increment $\Delta\zeta_e$ equal to 10% (being the latter the minimum requirement for a seismic improvement of residential buildings according to D.M. 2018), for all sites and number of storeys (Figure 13).

CONCLUSIONS

Pre-1970 reinforced concrete buildings are commonly susceptible to seismic loads worldwide, and many buildings in Italy were designed to sustain only gravity loads despite being in high seismic hazard areas. To reduce their vulnerabilities, it is important to carefully assess their seismic performance by analyzing typical failures exhibited after past earthquakes and implementing efficient retrofitting strategies.

In this study, seismic assessment and retrofitting of pre-70 RC building case-studies in Italy were conducted through simulated designs and pushover analyses using 3D models in OpenSees.

The safety check highlighted a significant vulnerability to shear failures, particularly in beam-column joints, which were often characterized by tensile failure.

A retrofit intervention was designed using pre-stressed steel strips to solve tensile failures in joints and FRP wrapping for beams/columns against shear failure. The effectiveness of the retrofit technique was found to be more limited for taller buildings, as joint compression failure is often difficult to solve without changing lateral stiffness. However, on average, retrofitted buildings can achieve 100% of the seismic capacity of a new building at SD LS if the PGA demand is less than 0.15 g, and 60% of this "target" performance if the demand is less than 0.25 g.

Based on the seismic safety evaluation conducted both before and after the retrofit intervention on all Italian municipalities analyzed in the article, functional laws were derived. These are able to provide, for a building similar to those considered in the study (both in terms of geometry and construction period) and for a given number of floors (i.e., 3 or 6), the expected value of the *ante-operam* safety index, the expected index improvement by implementing local interventions, and therefore also the average *post-operam* safety index. These functional laws provide important indications both on the pre-intervention health status of the building and on the potential benefits of a local intervention, based solely on seismic demand (i.e., PGA_D).

REFERENCES

[1] De Risi, M. T., Di Domenico, M., Manfredi, V., Terrenzi, M., Camata, G., Mollaioli, F., ... & Verderame, G. M. (2022a). Modelling and seismic response analysis of Italian pre-code and low-code reinforced concrete buildings. Part I: Bare frames. Journal of Earthquake Engineering, 1-32.

[2] Dolce, M., Speranza, E., De Martino, G., Conte, C., & Giordano, F. (2021). The implementation of the Italian National Seismic Prevention Plan: A focus on the seismic upgrading of critical buildings. International Journal of Disaster Risk Reduction, 62, 102391.

[3] D.M. 2018, Aggiornamento delle «Norme Tecniche per le Costruzioni» - D.M. 17/1/18. (in Italian)

[4] EN 1998-3-1-4. CEN (2005), Eurocode 8 - Design of Structures for Earthquake Resistance, Part 3, Assessment and Retrofitting of Buildings. European Committee for Standardization.

[5] ISTAT (2011) Istituto Nazionale di Statistica (National Institute of Statistics). 15° Censimento generale della popolazione e delle abitazioni. Dati sulle caratteristiche strutturale della popolazione, delle abitazioni e variabili (2011). (in Italian)

[6] R.D. Regio Decreto Legge n. 2229 del 16/11/1939. Norme per la esecuzione delle opere in conglomerate cementizio semplice od armato. G.U. n. 92 del 18/04/1940 (in Italian)

[7] Verderame, G.M., Polese, M., Mariniello, C., Manfredi, G., (2010). A simulated design procedure for the assessment of seismic capacity of existing reinforced concrete buildings. Advances in Engineering Software, 41(2), 323-335.

[8] Verderame, G.M., Ricci, P., Esposito, M., Manfredi, G., (2012). STIL v1.0 - Software per la caratterizzazione delle proprietà meccaniche degli acciai da c.a. tra il 1950 e il 2000. ReLUIS, http://www.reluis.it/

[9] De Risi M.T., Ricci P., Verderame G.M., (2022b). Experimental Analysis of the Effectiveness of Pre-Stressed Steel Strips for the Strengthening of Beam-Column Joints in Existing RC Buildings, XIX ANIDIS Conference, Seismic Engineering in Italy, September 2022, Torino, Italy.

[10] Fajfar, P. (2000). A nonlinear analysis method for performance-based seismic design. Earthquake spectra, 16(3), 573-592.

[11] Mori F, Mendicelli A, Moscatelli M, Romagnoli G, Peronace E, Naso G (2020). A new VS30 map for Italy based on the seismic microzonation dataset. Eng Geol 275:1–10.

[12] Biskinis, D., & Fardis, M. N. (2010). Flexure-controlled ultimate deformations of members with continuous or lap-spliced bars. Structural concrete, 11(2), 93-108.

[13] Circolare del Ministero dei Lavori Pubblici n. 65 del 10/4/1997 (1997) Istruzioni per l'applicazione delle "Norme tecniche per le costruzioni in zone sismiche" di cui al Decreto Ministeriale 16 gennaio 1996. G.U. n. 97 del 28/4/1997 (in Italian)

[14] McKenna, F. (2011). OpenSees: a framework for earthquake engineering simulation. Computing in Science & Engineering, 13(4), 58-66.

[15] Verderame, G. M., & Ricci, P. (2018). An empirical approach for nonlinear modelling and deformation capacity assessment of RC columns with plain bars. Engineering Structures, 176, 539-554.

[16] Vidic, T., Fajfar, P., & Fischinger, M. (1994). Consistent inelastic design spectra: strength and displacement. Earthquake Engineering & Structural Dynamics, 23(5), 507-521.

[17] Tsonos A.G., 2014. An innovative solution for strengthening of old R/C structures and for improving the FRP strengthening method. Structural Monitoring and Maintenance, 1(3), 323-338.

[18] Del Vecchio, C., Di Ludovico, M., Prota, A., & Manfredi, G. (2015). Analytical model and design approach for FRP strengthening of non-conforming RC corner beam–column joints. Engineering Structures, 87, 8-20.

[19] Pohoryles, D. A., Melo, J., Rossetto, T., D'Ayala, D., & Varum, H. (2018). Experimental comparison of novel CFRP retrofit schemes for realistic full-scale RC beam–column joints. Journal of Composites for Construction, 22(5), 04018027.

[20] De Risi, M. T., Del Vecchio, C., Ricci, P., Di Ludovico, M., Prota, A., & Verderame, G. M. (2020b). Light FRP Strengthening of Poorly Detailed Reinforced Concrete Exterior Beam–Column Joints. Journal of Composites for Construction, 24(3), 04020014.

[21] Verderame, G. M., Ricci, P., De Risi, M. T., & Del Gaudio, C. (2022). Experimental assessment and numerical modelling of conforming and non-conforming RC frames with and without infills. Journal of Earthquake Engineering, 26(2), 573-614.

[22] Dolce M., Gigliotti R., Laterza M., Nigro D., Marnetto R., 2001a. Il rafforzamento dei pilastri in c.a. mediante il sistema CAM. Atti del X Convegno ANIDIS "L'ingegneria sismica in Italia", September 9-13, Potenza-Matera, Italy. Paper F3-01. (in Italian)

[23] Dolce, M., Nigro, D., Ponzo, F.C., Marnetto, R., 2001b. Rafforzamento delle strutture murarie: il sistema CAM di Cuciture Attive per la Muratura. Atti del X Convegno ANIDIS "L'ingegneria sismica in Italia", September 9-13, Potenza-Matera, Italy. Paper E3-07. (in Italian)

[24] CNR-DT 200/2004. Istruzioni per la Progettazione, l'Esecuzione ed il Controllo di Interventi di Consolidamento Statico mediante l'utilizzo di Compositi Fibrorinforzati. (in Italian)